Global Biogeochemical Cycles

Supporting Information for

Stable Carbon Isotopes Suggest Large Terrestrial Carbon Inputs to the Global Ocean

Eun Young Kwon[1,2]*, Tim DeVries[3,4], Eric Galbraith[5,6]†, Jeomshik Hwang[7],

Guebuem Kim[7], and Axel Timmermann[1,2]

[1] Center for Climate Physics, Institute for Basic Science, Busan, 46241, South Korea

[2] Pusan National University, Busan, 46241, South Korea

[3] Department of Geography, University of California, Santa Barbara, CA 93106, USA

[4] Earth Research Institute, University of California, Santa Barbara, CA 93106, USA

[5] ICREA, Pg. Lluís Companys 23, 08010 Barcelona, Spain

[6] Institut de Ci encia i Tecnologia Ambientals (ICTA) and Department of Mathematics, Universitat Autonoma de Barcelona, 08193 Barcelona, Spain

[7] School of Earth and Environmental Sciences/Research Institute of Oceanography, Seoul National University, Seoul, 08826, South Korea

†Now at Earth and Planetary Science, McGill University, 450 University Street, Montreal, H3A 0E8, Canada

Contents of this file

Introduction

This Supplementary Information provides supplementary texts, figures and tables.

Supplementary Text 1. The Carbon Cycle Model

The oceanic ^{13}C is a prognostic variable in the model, and the $\delta^{13}C$ of DIC is calculated using the simulated $DI^{13}C$ and $DI^{12}C$. We briefly describe the $DI^{12}C$ and $DI^{13}C$ model formulations and identify the parameters to be optimized.

The governing equation for the $DI^{12}C$ model is

$$\frac{\partial[\mathrm{DI}^{12}\mathrm{C}]}{\partial t} + U \cdot \nabla[\mathrm{DI}^{12}\mathrm{C}] - \nabla(K\nabla[\mathrm{DI}^{12}\mathrm{C}]) = Jv_{DI^{12}C} + Jg_{DI^{12}C} + Jb_{DI^{12}C} + Jt_{DI^{12}C} + Jl_{DI^{12}C}, \quad \text{(S1)}$$

where the three terms on the left-hand side represent the time rate of change in $DI^{12}C$, and the advective and mixing processes of $DI^{12}C$. The five terms on the right-hand side represent the concentrating and diluting effect due to evaporation and precipitation (*Jv*), the air-sea gas exchange (*Jg*), the biological source and sink (*Jb*), the terrestrial carbon inputs to the ocean (*Jt*), and the sedimentary burial loss (*Jl*). The gas exchange term is expressed as

$$Jg_{DI^{12}C} = -(1 - Fice) \cdot k_g \cdot {z_0}^{-1} \cdot \left([^{12}\mathrm{CO}_2] - [^{12}\mathrm{CO}_2^{\mathrm{sat}}]\right), \quad \text{(S2)}$$

where *Fice* is a fraction of sea surface covered by sea ice, $z_0 = 36$ m is the thickness of the ocean top layer in the model, and $[^{12}CO_2]$ is simulated aqueous $^{12}CO_2$ concentration at the sea-surface and $[^{12}CO_2{}^{sat}]$ is saturated aqueous $^{12}CO_2$ concentration, the latter that is computed by multiplying the atmospheric pCO_2 (in μatm) with the solubility of CO_2 in seawater k_0 (in mol m^{-3} μatm^{-1}). The air-sea CO_2 transfer velocity k_g (in ms^{-1}) is formulated following an equation (Wanninkhof, 1992) adopted in the second phase of the Ocean Carbon Model Intercomparison Project (OCMIP2) protocol (Najjar et al., 2007) as

$$k_g = f1 \cdot \overline{u^2} \cdot (Sc/660)^{-1/2}, \quad \text{(S3)}$$

where *f1* is a linear scaling factor for the CO_2 transfer velocity to be optimized, *u* is the wind speed, an overbar represents a temporal average, and *Sc* is the Schmidt number. In Najjar et al. (2007), Wanninkhof (1992), and also in this study except in the "Gasx.exponent" experiment where we use the daily mean windspeed (u) instead of the monthly mean ($\bar{u}$), $\overline{u^2}$ is computed as $\bar{u}^2 + var$ where *var* represents the variance of wind speed over a month.

The biological source and sink terms are based on the OCMIP2 protocol (Najjar et al., 2007), and composed of the biological production and remineralization of organic carbon (OC) and $CaCO_3$ as

$$Jb_{DI^{12}C} = Jb_{O^{12}C} + Jb_{Ca^{12}CO3}. \quad \text{(S4)}$$

We refer the reader to Kwon and Primeau (2008) for the detailed descriptions of the *Jb* terms and the biogeochemical model formulations. The *Jb* term is important for bringing our simulated tracer distributions close to observations. Therefore, we optimize the model parameters governing the biological source and sink terms against observed PO_4, alkalinity, and $DI^{12}C$ using the same method employed in Kwon and Primeau (2008).

The terrestrial carbon input *Jt* term includes dissolved organic carbon (DOC) fluxes from rivers, particulate organic carbon (POC) fluxes from rivers and aerosols, and DIC fluxes from rivers and coastal margins as follows:

$$Jt_{DI^{12}C} = \frac{1}{\tau} \cdot [\mathrm{DOCr}] + Jt_{POC} + Jt_{DIC}, \quad \text{(S5)}$$

where DOCr is DOC derived from rivers, τ is the lifetime of DOCr and fixed at 8 years (Manizza et al., 2009) or 2 years (Anderson et al., 2019), and Jt_{POC} combines the riverine and aerosol driven POC fluxes, assumed to be remineralized instantaneously to DIC at the ocean bottom layer of the river mouths and the aerosol deposition sites, respectively. DOCr is the solution of the equation of

$$\frac{\partial[\mathrm{DOCr}]}{\partial t} + U \cdot \nabla[\mathrm{DOCr}] - \nabla(K\nabla[\mathrm{DOCr}]) = Jt_{DOC} - \frac{1}{\tau} \cdot [\mathrm{DOCr}], \quad \text{(S6)}$$

where Jt_{DOC} is riverine DOC flux. Jt_{DOC} and Jt_{POC} are prescribed using the Global Nutrient Export from Watersheds (NEWS2) model (Mayorga et al., 2010) for riverine fluxes and the atmospheric model

constrained by observations (Lamarque et al., 2010) for aerosol driven fluxes. Jt_{DIC} includes DIC fluxes from rivers (Jt_{DIC_river}) and coastal margins (Jt_{DIC_CM}), the latter including fluxes through SGD and direct lateral inputs from coastal vegetation. While riverine DIC fluxes are prescribed using the GEMS-GLORI database (Meybeck & Ragu, 2012), the magnitude and geographic distributions for the coastal margin DIC inputs are highly uncertain. Thus, Jt_{DIC_CM} is parameterized as

$$Jt_{DIC\_CM} = (f2 + f3 \cdot growth\ scale) \cdot fCM, \quad \text{(S7)}$$

where *fCM* is a globally uniform DIC flux within the top 217 m around the global coastlines except Antarctica, *growth scale* is a linear adjustment of the atmospheric growth of CO_2 increasing from 0 in 1780 to 0.44 in 2016. The *growth scale* is parameterized using the estimated CO_2 emissions from land use change (Friedlingstein et al., 2019) in the "Landusescale" experiment. The two tunable parameters *f2* and *f3* determine the magnitude of preindustrial and industrial coastal margin carbon fluxes. In the "Basin" experiment described in Section 4.5, instead of specifying a globally-uniform value for *f2* in Equation (S7), we specify three separate *f2* values (i.e., *f2.arc-atl*, *f2.pac* and *f2.ind*) that represent the coastal margin carbon fluxes in three separate basins (Arctic-Atlantic, Pacific, and Indian). Once discharged to the ocean, the coastal margin DIC mixes with oceanic DIC and undergoes transport by ocean circulations, air-sea CO_2 exchange, biological cycling, and sedimentary burial.

The sedimentary burial flux *Jl* term is parameterized using another parameter *f4* as

$$Jl_{DI^{12}C} = \begin{cases} -f4 \cdot fburial & \text{where } \Omega \geq 1 \\ 0 & \text{where } \Omega < 1 \end{cases}, \quad \text{(S8)}$$

where *fburial* is a uniform DIC sink from the ocean bottom layer, and the saturation state of seawater with respect to calcite, Ω, is determined using the GLODAPv2 dataset (Lauvset et al., 2016).

In the following, we describe our $DI^{13}C$ model equations. The governing equation for $DI^{13}C$ can be written as

$$\frac{\partial[\mathrm{DI}^{13}\mathrm{C}]}{\partial t} + U \cdot \nabla[\mathrm{DI}^{13}\mathrm{C}] - \nabla(K\nabla[\mathrm{DI}^{13}\mathrm{C}]) = Jv_{DI^{13}C} + Jg_{DI^{13}C} + Jb_{DI^{13}C} + Jt_{DI^{13}C} + Jl_{DI^{13}C}, \quad \text{(S9)}$$

where $Jb_{DI^{13}C} = Jb_{O^{13}C} + Jb_{Ca^{13}CO3}$. The virtual flux term ($Jv_{DI^{13}C}$) only redistributes surface $DI^{13}C$, the same way as ocean circulations do. Hence, the virtual flux term can be treated as the ocean transport term on the left-hand side, representing the convergence and divergence of $DI^{13}C$ due to ocean circulations and air-sea freshwater fluxes.

The fractionation during air-sea gas exchange is expressed as

$$Jg_{DI^{13}C} = -f1 \cdot \frac{k_g}{z_0} \alpha_k \left(\alpha_{aq \leftarrow DIC} \cdot \frac{[DI^{13}C]}{[DI^{12}C]} \cdot [^{12}CO_2] - \alpha_{aq \leftarrow g} \cdot \frac{^{13}CO_2^{air}}{^{12}CO_2^{air}} \cdot [^{12}CO_2^{sat}] \right), \quad \text{(S10)}$$

where α_k is the kinetic fractionation factor, $\alpha_{aq \leftarrow DIC}$ is the fractionation factor from DIC to aqueous CO_2, $\alpha_{aq \leftarrow g}$ is the fractionation factor from gaseous CO_2 to aqueous CO_2, and CO_2^{air} is atmospheric CO_2 concentration. The kinetic fractionation factor and the fractionation factor from gaseous to aqueous CO_2 are fixed at α_k=0.99915 and $\alpha_{aq \leftarrow g}$ =0.998764, respectively (Schmittner et al., 2013). The fractionation factor $\alpha_{aq \leftarrow DIC}$ can be rewritten as $\alpha_{aq \leftarrow DIC} = \alpha_{aq \leftarrow g} / \alpha_{DIC \leftarrow g}$ with $\alpha_{DIC \leftarrow g} = 1.4 \times 10^{-5} \cdot T \cdot f_{CO3} - 1.05 \times 10^{-4} \cdot T + 1.01053$, where *T* is ocean temperature in °C and fco_3 is the fraction of CO_3^{2-} ions in DIC (Zhang et al., 1995).

The fractionation during the photosynthetic fixation of CO_2 is expressed as

$$Jb_{O^{13}C} = \alpha_{OC \leftarrow DIC} \cdot \frac{[DI^{13}C]}{[DI^{12}C]} \cdot Jb_{O^{12}C}, \quad \text{(S11)}$$

where $\alpha_{OC \leftarrow DIC}$ is the fractionation factor from DIC to organic carbon, which includes both particulate and dissolved organic carbon. The fractionation factor from DIC to organic carbon can be rewritten as $\alpha_{OC \leftarrow DIC} = \alpha_{OC \leftarrow aq} \cdot \alpha_{aq \leftarrow g} / \alpha_{DIC \leftarrow g}$ with $\alpha_{OC \leftarrow aq} = -0.00935 \cdot log_{10}([CO_2]) + 0.99626$ where $[CO_2]$ is aqueous CO_2 concentration in μmol l^{-1} after Goericke and Fry (1994). This parameterization gives the photosynthetic

fractionations from DIC to organic carbon ranging from -18‰ in low latitudes to -27‰ in high latitudes. There is no fractionation during the formation and dissolution of biogenic $CaCO_3$, and hence the $Jb_{Ca^{13}CO3}$ term becomes

$$Jb_{Ca^{13}CO3} = Jb_{Ca^{12}CO3} \cdot \frac{[DI^{13}C]}{[DI^{12}C]}. \quad \text{(S12)}$$

The $\delta^{13}C$ endmember values for terrestrial carbon are fixed at -27 ‰ for DOC, -30 ‰ for POC, and -15 ‰ for riverine DIC (Marwick et al., 2015; Peterson & Fry, 1987). For the coastal margin carbon flux, we parameterize the $\delta^{13}C$ endmember value as $\delta^{13}C\_CM = f5 + f6 \cdot growth\ scale$. The term representing terrestrial $DI^{13}C$ inputs becomes

$$Jt_{DI^{13}C} = 0.973 \cdot \frac{1}{\tau} \cdot [DOCr] + 0.970 \cdot Jt_{POC} + 0.985 \cdot Jt_{DIC_{river}} + (1 + \delta^{13}\text{C\_CM}\ /1000) \cdot Jt_{DIC\_CM}. \quad \text{(S13)}$$

Fractionation does not occur during the sedimentary burial of $DI^{13}C$, hence

$$Jl_{DI^{13}C} = \begin{cases} -f4 \cdot fburial \cdot \frac{[DI^{13}C]}{[DI^{12}C]} & \text{where } \Omega \geq 1 \\ 0 & \text{where } \Omega < 1 \end{cases}. \quad \text{(S14)}$$

In the "Standard" model, we optimize the parameter values for f1 to f6 simultaneously using observations.

Supplementary Text 2. Sensitivity Experiments and Additional Model Caveats

Here we explore the sensitivity of our optimization results to some of model setups and assumptions using a series of sensitivity experiments with the optimization model, which are summarized and compared to the results of the "Standard" model (presented in the main text) in Table S1. We also discuss some caveats of the model that could lead to additional uncertainties in our inferred carbon fluxes.

2.1 Sensitivity to Ocean Temperatures for Simulating Carbon Isotopes

We explore how model SST influences our results through the effects of CO_2 solubility and carbon isotope fractionations. To this end, we perform three experiments where we use different SST fields for the temperature-dependent equilibrium fractionation during air-sea CO_2 exchange ($\alpha_{DIC \leftarrow g}$) and the solubility of CO_2 in seawater. In the "Mod.SST" experiment, we use the model SST for the equilibrium fractionation factor and the solubility. In the "HadI.solubility" experiment, we force a correction for the model SST cold bias by replacing the model SST with the annual mean SST from the Met Office Hadley Centre's sea ice and sea surface temperature dataset (HadISST) (Rayner et al., 2003) when calculating the equilibrium fractionation factor and the solubility. In the "Standard" experiment, we use the HadISST (Rayner et al., 2003) when calculating the equilibrium fractionation factor, while keeping the model SST for the solubility of CO_2. While SST is assumed to be time-invariant in the "Mod.SST" experiment, we use time-varying SST for simulations of 1870-2016 and a time-invariant SST averaged over the first 50 years for simulations of 1780-1869 in the "HadI.solubility" and "Standard" experiments.

The estimated coastal margin carbon inputs are 0.9±0.3 GtC/yr in the "Mod.SST" setup, 0.8±0.2 GtC/yr in the "standard" setup, and 1.1±0.2 GtC/yr in the "HadI.solubilty" setup. The estimated $\delta^{13}C$ values for the coastal margin fluxes are more spread with -31±6‰ for the "Mod.SST" setup, -22±5‰ for the "HadI.solubility" setup, and -26±5‰ for the "Standard" setup. The CO_2 gas transfer velocity is similar in the three setups, while the sedimentary burial of inorganic carbon is smallest in the HadI.solubility experiment (Table S1). Overall the coastal margin carbon inputs are not highly sensitive

to the SST used in the model, but resolving the seasonal cycle in SST would help to more precisely determine the magnitude and $\delta^{13}C$ value of the coastal margin inputs.

2.2 Sensitivity to Organic Carbon Burial in Marine Sediments

A missing component in the model is the burial of terrestrially-derived organic carbon, which is estimated to be 0.1-0.2 GtC/yr globally, and which occurs mostly on continental shelves and slopes (Bianchi et al., 2017; Cai, 2011). Because this burial flux occurs in the same coastal regions where terrestrial inputs occur, and it has the same isotopic signature as the terrestrial inputs, we cannot independently constrain both the input fluxes and subsequent burial of terrestrially-derived organic carbon. Thus, our estimated terrestrial carbon fluxes represent the residual between the total input of terrestrial carbon and its burial in coastal sediments. Nonetheless, there may also be significant burial of non-terrestrially-derived organic carbon in the ocean, which is also focused on continental shelves (Burdige, 2007), and may affect the carbon isotope balance. In order to explore the sensitivity of our results to the impact of organic carbon burial on the carbon isotope balance, we performed an experiment ("OC.burial") in which we optimized the $\delta^{13}C$ value of the carbon buried in marine sediments instead of fixing it at 0‰ (Table S1). The optimized carbon burial fluxes are 0.18±0.05 GtC/yr with a $\delta^{13}C$ signature of -4±2‰. This implies that about 16% of the carbon burial occurs in a form of organic carbon, if the $\delta^{13}C$ value of the organic carbon is -25‰. In this experiment, we obtain a coastal margin carbon input of 0.7±0.3 GtC/yr with a $\delta^{13}C$ value of -31±7‰, consistent with results from the "Standard" model within its uncertainty (Table S1).

Another caveat of our study is that we assume a steady-state balance between terrestrial carbon inputs and the burial and outgassing of inorganic carbon. If there are long-term imbalances between carbonate weathering and burial fluxes (Cartapanis et al., 2018; Milliman, 1993), or imbalances between sedimentary burial of marine organic matter (Burdige, 2007) and carbon fluxes from underwater seeps, vents, and volcanoes (Reeburg, 2007), these imbalances could add additional uncertainty to our estimated terrestrial carbon inputs and associated carbon fluxes. If sedimentary burial fluxes of marine organic carbon exceed the supplies from seeps, vents, and volcanoes in the present-day ocean, as suggested by Cartapanis et al. (2018), then our method would underestimate the total terrestrial carbon inputs to the global ocean, while the opposite would be true if the supply exceeds sedimentary burial fluxes. Nonetheless, these imbalances are likely small (on the order of 0.1 GtC/yr) (Cartapanis et al., 2018), and would not affect our results substantially.

As a test, we run a transient simulation by imposing a globally-uniform DIC sink with a $\delta^{13}C$ value of -12.5‰, which is not balanced by terrestrial carbon inputs. The transient DIC sink is imposed at the ocean bottom layer of all coastal grid cells (Figure S2c) except those surrounding Antarctica. The prescribed DIC sink rate is uniformly distributed such that the globally-integrated value becomes 0.3 GtC/yr. By prescribing the $\delta^{13}C$ value at -12.5‰, we are assuming that the 0.3 GtC/yr of carbon burial includes organic carbon burial of 0.15 GtC/yr with $\delta^{13}C$ = -25‰ and inorganic carbon burial of 0.15 GtC/yr with $\delta^{13}C$ = 0‰. For this experiment, we integrate the preindustrial state of the "Standard" model over 1000 years with the imposed transient DIC sink while allowing for temporal drifts in oceanic carbon reservoirs. The 1000-year simulation mimics a temporal drift in the inventory and distributions of carbon isotopes under a preindustrial atmospheric condition from a year of 780 to 1779. The model is then integrated from 1780 to 2016 with the observed historical atmospheric CO_2 forcing with the same DIC sink. This simulation results in a RMSE of 21 $\mu molkg^{-1}$ for DIC and 0.19 ‰ for the $\delta^{13}C$ of DIC. The model-observation mismatch for DIC is relatively larger than the case in the "Standard" experiment. Yet, the consideration of a temporal imbalance between carbon burial fluxes and inputs is unlikely to change our conclusions given a good agreement in the observed $\delta^{13}C$ of DIC.

In all, the carbon burial fluxes estimated in this study are relatively weakly constrained, and could contribute an additional uncertainty of up to 0.2 GtC/yr (Cai, 2011; Cartapanis et al., 2018) to our carbon budget. We therefore apply an uncertainty of 0.3 GtC/yr to our estimated carbon burial fluxes in our final budget (Figure 10).

2.3 Sensitivity to the Relationship between Wind-Speed and Air-Sea CO_2 Exchange Rate

The air-sea exchange and oceanic distributions of carbon isotopes are sensitive to the relationship between air-sea CO_2 transfer velocity and winds, and Krakauer et al. (2006) derived a linear relationship using observed isotope distributions in the ocean and atmosphere. In order to explore the sensitivity of our results to the relationship, we perform the "Gasx.exponent" experiment (Table S1) by adding one more degree of freedom to the air-sea CO_2 exchange parameterization (k_g in Equation (S3)) as

$$k_g = f1.linear \cdot \overline{u^{f1.exp}} \cdot (Sc/660)^{-1/2}, \quad \text{(S15)}$$

where $f1.linear$ is a linear scaling parameter to the CO_2 transfer velocity, $f1.exp$ is an exponent to the daily mean wind speed *u* from the ERA-Interim reanalysis (Dee et al., 2011). Our optimization results suggest that the optimal value for *f1.exp* is 2.01±0.05, supporting an earlier finding that a quadratic relationship is appropriate for the large-scale CO_2 fluxes within the range of observed wind speed (Wanninkhof et al., 2009). The resulting estimate for the globally-averaged air-sea CO_2 transfer velocity of 15.1±1.3 cm/hr coincides with the optimal value from the "Standard" experiment, and also is consistent with latest estimates of 14-17 cm/hr constrained using the quadratic relationship (Graven et al., 2012; Naegler et al., 2006; Sweeney et al., 2007; Wanninkhof et al., 2013). The other model estimates also remain consistent with those from the "Standard" experiment within the uncertainty ranges (Table S1).

2.4 Sensitivity to the $\delta^{13}C$ values of terrestrial carbon

While potential uncertainties in the prescribed riverine $\delta^{13}C$ values of ±2‰ (Table 1) are taken into consideration in our Monte Carlo experiments, it is still unclear how those uncertainties might affect our results in an optimization framework. In order to explore the sensitivity of our estimated terrestrial carbon inputs to the $\delta^{13}C$ values prescribed for riverine carbon inputs, we deviate the prescribed $\delta^{13}C$ values for riverine DOC, POC, and DIC fluxes by ±5‰ and optimize two key parameters representing the preindustrial coastal margin flux and the $\delta^{13}C$ value for the coastal margin flux. The other model parameters are all fixed at their optimal values obtained from the "Standard" experiment (Table S1) for the computational efficiency. The results from the suite of experiments are summarized in Table S2, which essentially shows that any uncertainties associated with the prescribed $\delta^{13}C$ values for riverine carbon fluxes propagate into the uncertainty in the estimated $\delta^{13}C$ value for the coastal margin flux, not the estimated coastal margin flux. With the large ranges of the prescribed $\delta^{13}C$ values for riverine carbon fluxes of -27±5‰ for DOC, -30±5‰ for POC, and -15±5‰ for riverine DIC, our optimized coastal margin $\delta^{13}C$ values are in the range of -26±4‰, which is within our estimated uncertainty in the "Standard" experiment. The influence of the covariations between the magnitude and isotopic composition of the coastal margin inputs on our results are explored in the main text (Figures 9a and 9b).

2.5 Industrial changes in land-originated carbon

Another simplification in our model is our assumption of time-invariant riverine carbon inputs, and coastal margin inputs whose industrial evolutions are linearly scaled with atmospheric CO_2. To explore a sensitivity of our results to an alternative scaling, we run another optimization by assuming that the industrial evolution of the coastal margin input is linearly scaled with the CO_2 emissions from land-use change (Friedlingstein et al., 2019). The optimization results ("Landusescale" experiment in Table S1)

are the same as the ones from the "Standard" model, yielding a negligible perturbation during the industrial era. Nonetheless, it is possible that neither the atmospheric CO_2 nor the land-use change driven CO_2 emissions would be a good approximation for the historical changes in the coastal margin inputs, given our inability to reconstruct past changes in the area and density of coastal vegetations (Duarte, 2017). Nevertheless, those industrial evolutions in the coastal margin inputs and the $\delta^{13}C$ value are likely to emerge as anthropogenic perturbations in both DIC and the $\delta^{13}C$ of DIC (e.g., Figure 5), affecting the relatively well-ventilated portions of the global ocean only. These anthropogenically induced transient effects are quite distinct from the steady-state effects of the preindustrial coastal margin inputs (Figures 1g and 1h). Therefore, uncertainties in the industrial changes are unlikely to be an important source of uncertainty, at least for our estimates for the preindustrial coastal margin inputs.

2.6 Potential increases in coastal ocean productivity

We have not considered any anthropogenic perturbations to ocean productivity in this study, which could be particularly important to the carbon budget in the coastal oceans. Any potential increases in surface productivity in coastal regions, due to excess nutrient inputs from land, would have kept the coastal surface pCO_2 from rising, turning the coastal ocean to a greater sink of atmospheric CO_2 (Laruelle et al., 2018; Mackenzie et al., 2011). If this occurred on a global scale, the air-sea CO_2 exchange especially in coastal regions would have been modulated during industrial times. Although our model is not suitable to simulate anthropogenic increases in coastal ocean productivity, we carry out an idealized experiment where a transient increase in riverine PO_4 inputs is imposed over 1780-2016, while the other model parameters are held fixed at the values obtained from the "Standard" experiment. The anthropogenic increase in the land-originated PO_4 is assumed to be linearly scaled with an atmospheric growth of atmospheric CO_2 (Figure S2d). The linear scaling factor is arbitrarily determined such that the simulated DIC and the $\delta^{13}C$ of DIC are still optimal (RMSEs are 18 μmol kg^{-1} for DIC and 0.19‰ for the $\delta^{13}C$ of DIC in this idealized experiment). This experiment indeed shows that the increased coastal productivity, caused by the increased PO_4 supplies, leads to a weakening of coastal CO_2 efflux to the atmosphere by 0.1 GtC/yr as of 2000 (Figure S2e). Future studies should address more realistic features in the anthropogenic increases in nutrient and alkalinity supplies and the marine ecosystem responses to the perturbations. Nevertheless, the result shows that the model-observation disagreement in the coastal ocean air-sea CO_2 exchange does not necessarily indicate an overestimation of terrestrial carbon inputs to the ocean.

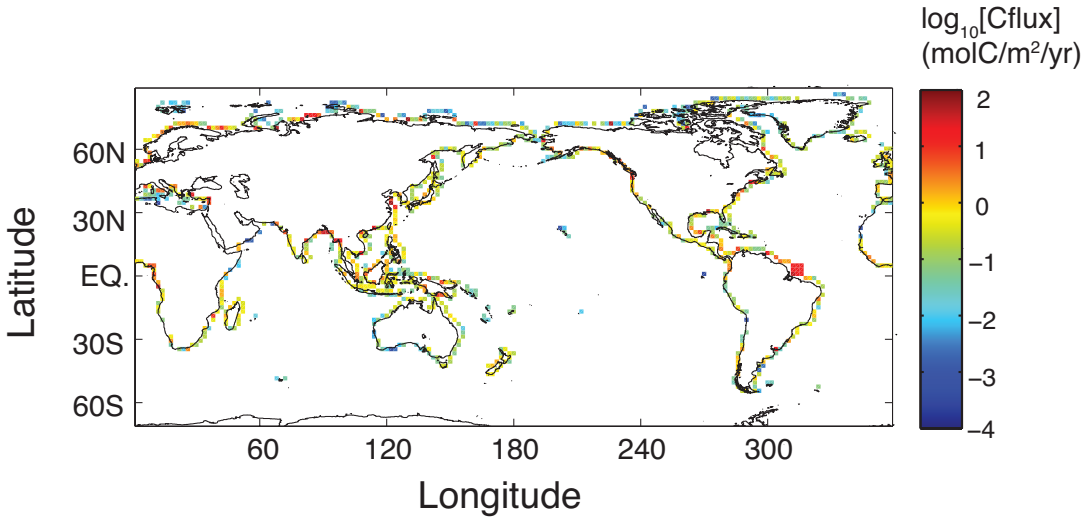

Figure S1. Prescribed riverine carbon inputs to the ocean, including POC and DOC fluxes based on Mayorga et al. (2010) and DIC fluxes based on Meybeck and Ragu (2012). A logarithmic scale with a base of 10 is used for the color scale. Unit is moles of carbon per a unit grid area per year.

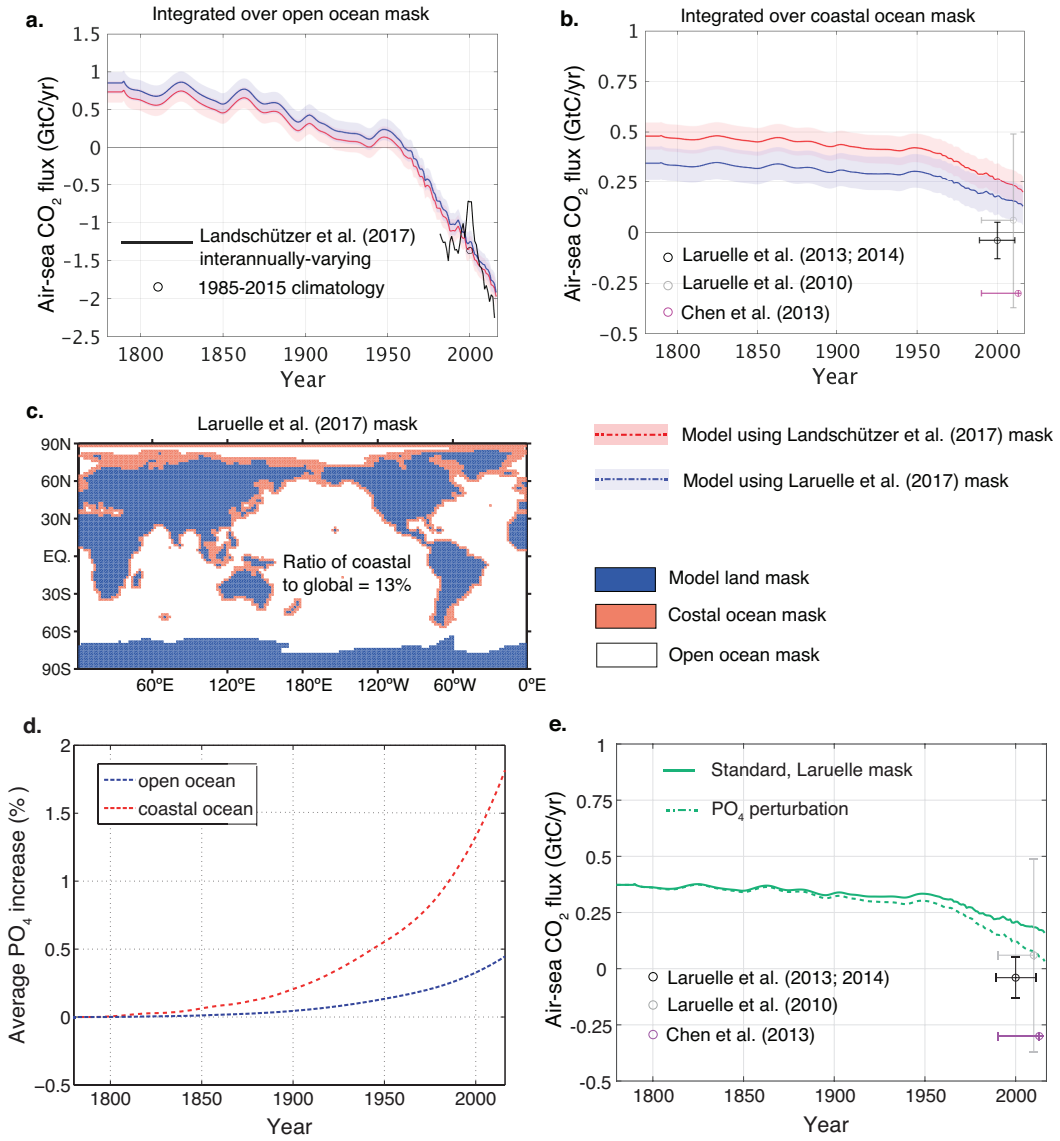

Figure S2. (a) Air-sea CO_2 fluxes from the "Standard" model are integrated over the open ocean using two different definitions for the coastal and open ocean. The red line with shading is from the definition used in Figure 4, while the blue line with shading is from Laruelle et al. (2017) where the coastal mask is defined as the ocean grid cells with isobaths less than 1000m or with distance from the coastline less than 300 km. The open ocean mask is the remaining ocean surface. Negative fluxes represent a net CO_2 uptake by the ocean while positive fluxes represent a net outgassing to the atmosphere. (b) Air-sea CO_2 fluxes integrated over the coastal masks. The black, gray, and magenta circles represent the observation-based estimates of -0.04±0.05 GtC/yr (Laruelle et al., 2013; Laruelle et al., 2014), 0.06±0.43 GtC/yr (Laruelle et al., 2010), and -0.3 GtC/yr (Chen et al., 2013), respectively. The time error bars for the gray and magenta circles are drawn assuming that their estimates were based on the past 20 years of observations. (c) The coastal and open ocean masks following Laruelle et al. (2017). (d and e) An idealized sensitivity experiment demonstrating the modulation of air-sea CO_2 fluxes due to increased PO_4 inputs from land. (d) Percentage increases in PO_4 concentrations as a function of time averaged over the coastal (red dashed line) and open ocean (blue dashed line) domains. (e) Air-sea CO_2 fluxes averaged over the coastal ocean. The green solid line is the same as the blue line in (b), while the green dashed line is from the idealized sensitivity experiment where the terrestrial PO_4 inputs have increased during industrial times.

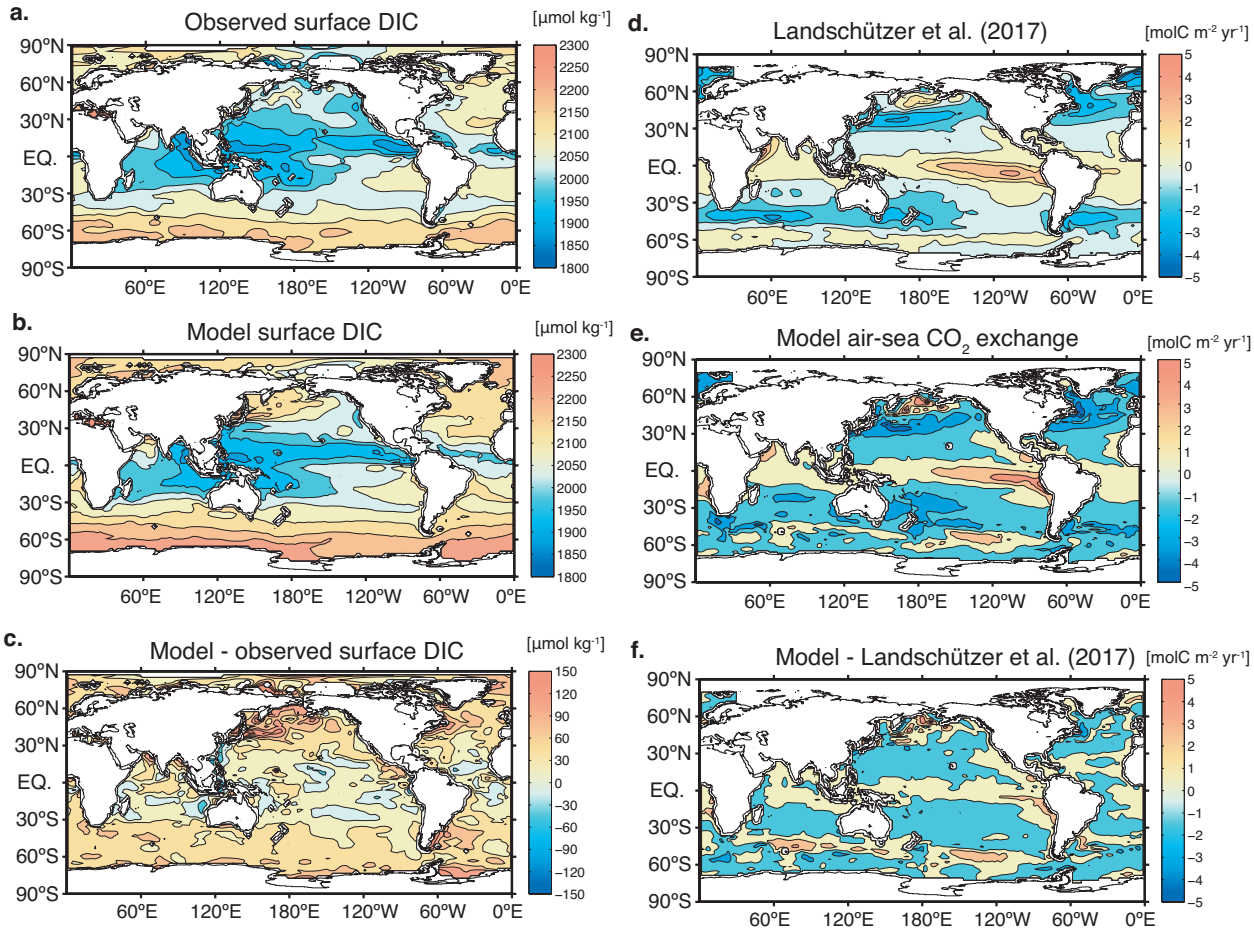

Figure S3. Comparison of surface DIC and air-sea CO_2 exchange between observations and the "Standard" model. (a) Observed surface DIC (Lauvset et al., 2016). (b) Surface DIC from the model. (c) The difference between the model and observed surface DIC. (d) Observation-based estimates for air-sea CO_2 exchange (Landschützer et al., 2017). Positive values represent CO_2 efflux to the atmosphere and negative values represent CO_2 uptake by the ocean. (e) Air-sea CO_2 exchange form the model. (f) The difference between the model and observed air-sea CO_2 exchange.

Table S1

Summary of Sensitivity Experiments (Red font indicates terms that are held fixed during the optimization and blue font indicates terms that are optimized).

[1]Experiments	RMSE_DIC (μmol/kg)	RMSE_$\delta^{13}C$ (‰)	Terrestrial C flux in 1780 (GtC/yr)	Terrestrial C flux in 2016 (GtC/yr)	[2]Gas transfer velocity (cm/hr)	[2]Inorganic carbon burial (GtC/yr)	$\delta^{13}C$ of coastal margin input in 1780 (‰)	$\delta^{13}C$ of coastal margin input in 2016 (‰)
Standard	18.2	0.19	1.4±0.2	1.4±0.2	15.1±2.5	0.22±0.06	-26±5	-26±5
Mod.SST	18.2	0.19	1.5±0.3	1.5±0.3	15.0±±1.0	0.22±0.04	-31±6	-31±6
HadI.solubility	17.0	0.19	1.7±0.2	1.7±0.2	15.1±2.4	0.05±0.08	-22±5	-22±5
Basin	17.7	0.18	1.4±0.1	[3]1.4±0.1	14.5±1.6	0.16±0.06	-27±4	[3]-27±4
OC.burial	17.9	0.19	1.3±0.3	[3]1.3±0.3	14.5±0.6	0.18±0.05	-31±7	[3]-31±7
Gasx.exponent	18.1	0.19	1.3±0.1	1.3±0.1	15.1±1.3	0.21±0.05	-25±2	[3]-25±2
Landusescale	18.2	0.19	1.4±0.2	1.4±0.2	15.1±2.5	0.22±0.06	-26±5	-26±5

[1] See the main text and Supplementary Text S2 for descriptions of the experiments
[2] Globally-averaged values based on the optimized parameters are shown
[3] A temporal scaling factor is set to zero so that there is no anthropogenic perturbation over time

Table S2. Sensitivity experiments to different $\delta^{13}C$ values prescribed for riverine carbon inputs. Multiple globally-uniform $\delta^{13}C$ values are prescribed for riverine carbon fluxes while optimizing the time-invariant coastal margin carbon input and the $\delta^{13}C$ value of the coastal margin carbon.

The $\delta^{13}C$ for prescribed riverine carbon flux			Optimization results			
$\delta^{13}C$_DOC (‰)	$\delta^{13}C$_POC (‰)	$\delta^{13}C$_DIC (‰)	RMSE_DIC (μmol/kg)	RMSE_$\delta^{13}C$ (‰)	Terrestrial C flux in 1780 (GtC/yr)	$\delta^{13}C$ of coastal margin input (‰)
-33	-35	-20	18.2	0.19	1.4	-23
		-15	18.2	0.19	1.4	-25
		-10	18.2	0.19	1.4	-27
	-30	-20	18.2	0.19	1.4	-24
		-15	18.2	0.19	1.4	-26
		-10	18.2	0.19	1.4	-28
	-25	-20	18.2	0.19	1.4	-25
		-15	18.2	0.19	1.4	-27
		-10	18.2	0.19	1.4	-28
-27	-35	-20	18.2	0.19	1.4	-24
		-15	18.2	0.19	1.4	-26
		-10	18.2	0.19	1.4	-28
	-30	-20	18.2	0.19	1.4	-25
		-15	18.2	0.19	1.4	-26
		-10	18.2	0.19	1.4	-27
	-25	-20	18.2	0.19	1.4	-26
		-15	18.2	0.19	1.4	-27
		-10	18.2	0.19	1.4	-29
-22	-35	-20	18.2	0.19	1.4	-25
		-15	18.2	0.19	1.4	-27
		-10	18.2	0.19	1.4	-28
	-30	-20	18.2	0.19	1.4	-26
		-15	18.2	0.19	1.4	-27
		-10	18.2	0.19	1.4	-29
	-25	-20	18.2	0.19	1.4	-26
		-15	18.2	0.19	1.4	-28
		-10	18.2	0.19	1.4	-30

References

Anderson, T. R., Rowe, E. C., Polimene, L., Tipping, E., Evans, C. D., Barry, C. D. G., Hansell, D. A., Kaiser, K., Kitidis, V., Lapworth, D. J., Mayor, D. J., Montheith, D. T., Pickard, A. E., Sanders, R. J., Spears, B. M., Torres, R., Tye, A. M., & Waska, H. (2019). Unified concepts for understanding and modelling turnover of dissolved organic matter from freshwaters to the ocean: the UniDOM model. *Biogeochemistry, 146*, 105-123. https://doi.org/10.1007/s10533-019-00621-1

Bianchi, D., Cui, X., Blair, N. E., Burdige, D. J., Eglinton, T., & Galy, V. (2017). Centers of organic carbon burial and oxidation at the land-ocean interface. *Org. Geochem.* https://doi.org/10.1016/j.orggeochem.2017.09.008

Burdige, D. J. (2007). Preservation of Organic Matter in Marine Sediments: Controls, Mechanisms, and an Imbalance in Sediment Organic Carbon Budgets? *Chem. Rev., 107*, 467-485.

Cai, W.-J. (2011). Estuarine and coastal ocean carbon paradox: CO2 sinks or sites of terrestrial carbon incineration? *Annu. Rev. Mar. Sci., 3*, 123-145.

Cartapanis, O., Galbraith, E. D., Bianchi, D., & Jaccard, S. (2018). Carbon burial in deep-sea sediment and implications for oceanic inventories of carbon and alkalinity over the last glacial cycle. *Clim. Past Discuss.* https://doi.org/10.5194/cp-2018-49

Chen, C.-T. A., Huang, T. H., Chen, Y.-C., Bai, Y., He, X., & Kang, Y. (2013). Air–sea exchanges of CO2 in the world's coastal seas. *Biogeosciences, 10*, 6509-6544. https://doi.org/10.5194/bg-10-6509-2013

Dee, D. P., Uppala, S. M., Simmons, A. J., Berrisford, P., Poli, P., S., K., Andrae, U., Balmaseda, M. A., Balsamo, G., Bauer, P., Bechtold, P., Beljaars, A. C. M., van de Berg, L., Bidlot, J., Bormann, N., Delsol, C., Dragani, R., Fuentes, M., Geer, A. J., & Haimberger, L. (2011). The ERA-Interim reanalysis: configuration and performance of the data assimilation system. *Q.J.R. Meteorol. Soc., 137*, 553-597.

Duarte, C. M. (2017). Reviews and syntheses: Hidden forests, the role of vegetated coastal habitats in the ocean carbon budget. *Biogeosciences, 14*, 301-310. https://doi.org/10.5194/bg-14-301-2017

Friedlingstein, P., Jones, M. W., O'Sullivan, M., Andres, R. M., Hauck, J., Peters, G. P., Peters, W., Pongratz, J., Sitch, S., Le Quéré, C., Bakker, D. C. E., & Canadell, J. (2019). Global Carbon Budget 2019. *Earth Syst. Sci. Data, 11*, 1783-1838. https://doi.org/10.5194/essd-11-1783-2019

Goericke, R., & Fry, B. (1994). Variations of marine plankton $\delta^{13}C$ with latitude, temperature, and dissolved CO_2 in the world ocean. *Global Bigeochem. Cycles, 8*, 85-90.

Graven, H. D., Gruber, N., Key, R., Khatiwala, S., & Giraud, X. (2012). Changing controls on oceanic radiocarbon: New insights on shallow-to-deep ocean exchange and anthropogenic CO_2 uptake. *J. Geophys. Res., 117*, C10005. https://doi.org/10.1029/2012JC008074

Krakauer, N. Y., Randerson, J. T., Primeau, F. W., Gruber, N., & D., M. (2006). Carbon isotope evidence for the latitudinal distribution and wind speed dependence of the air-sea gas transfer velocity. *Tellus, 58B*, 390-417.

Kwon, E. Y., & Primeau, F. (2008). Optimization and sensitivity of a global biogeochemistry ocean model using combined in situ DIC, alkalinity, and phosphate data. *J. Geophys. Res., 113*(C08011). https://doi.org/10.1029/2007JC004520

Lamarque, J. F., Bond, T. C., Eyring, V., Granier, C., Heil, A., Klimont, Z., Lee, D., Liousse, C., Mieville, A., Owen, B., Schultz, M. G., Shindell, D., Smith, S. J., Stehfest, E., Van Aardenne, J., Cooper, O. R., Kainuma, M., Mahowald, N., McConnell, J. R., Naik, V., Riahi, K., & van Vuuren, D. P. (2010). Historical (1850–2000) gridded anthropogenic and biomass burning emissions of reactive gases and aerosols: methodology and application. *Atmospheric Chemistry and Physics, 10*(15), 7017-7039. https://doi.org/10.5194/acp-10-7017-2010

Landschützer, P., Gruber, N., & Bakker, D. C. E. (2017). *An updated observation-based global monthly gridded sea surface pCO_2 and air-sea CO_2 flux product from 1982 through 2015 and its monthly climatology (NCEI Accession 0160558)* Version 2.2) NOAA National Centers for Environmental Information.

Laruelle, G. G., Cai, W.-J., Hu, X., Gruber, N., Mackenzie, F. T., & Regnier, P. (2018). Continental shelves as a variable but increasing global sink for atmospheric carbon dioxide. *Nature Communications, 9*(454). https://doi.org/10.1038/s41467-017-02738-z

Laruelle, G. G., Dürr, H. H., Lauerwald, R., Hartmann, J., Slomp, C. P., Goossens, N., & Regnier, P. A. G. (2013). Global multi-scale segmentation of continental and coastal waters from the watersheds to the continental margins. *Hydrology and Earth System Sciences, 17*(5), 2029-2051. https://doi.org/10.5194/hess-17-2029-2013

Laruelle, G. G., Dürr, H. H., Slomp, C. P., & Borges, A. V. (2010). Evaluation of sinks and sources of CO_2 in the global coastal ocean using a spatially-explicit typology of estuaries and continental shelves. *Geophys. Res. Lett., 37*(L15607). https://doi.org/10.1029/2010GL043691

Laruelle, G. G., Landschutzer, P., Gruber, N., Tison, J.-L., Delille, B., & Regnier, P. (2017). Global high-resolution monthly pCO_2 climatology for the coastal ocean derived from neural network interpolation. *Biogeosciences, 14*, 4545-4561.

Laruelle, G. G., Lauerwald, R., Pfeil, B., & Regnier, P. (2014). Regionalized global budget of the CO_2 exchange at the air-water interface in continental shelf seas. *Global Bigeochem. Cycles, 28*, 1194-1214. https://doi.org/10.1002/2014GB004832

Lauvset, S. K., Key, R. M., Olsen, A., van Heuven, S., Velo, A., Lin, X., Schirnick, C., Kozyr, A., Tanhua, T., Hoppema, M., Jutterström, S., Steinfeldt, R., Jeansson, E., Ishii, M., Perez, F. F., Suzuki, T., & Watelet, S. (2016). A new global interior ocean mapped climatology: the 1° × 1° GLODAP version 2. *Earth System Science Data, 8*(2), 325-340. https://doi.org/10.5194/essd-8-325-2016

Mackenzie, F. T., Lerman, A., & DeCarlo, E. H. (2011). Coupled C, N, P, and O biogeochemical cycling at the land-ocean interface. In J. Middleburg & R. Laane (Eds.), *Treatise on Ocean and Estuarine Science*. Elsevier.

Manizza, M., Follows, M. J., Dutkiewicz, S., McClelland, J. W., Menemenlis, D., Hill, C. N., Townsend-Small, A., & Peterson, B. J. (2009). Modeling transport and fate of riverine dissolved organic carbon in the Arctic Ocean. *Global Biogeochemical Cycles, 23*(GB4006). https://doi.org/10.1029/2008GB003396

Marwick, T. R., Tamooh, F., Teodoru, C. R., Borges, A. V., Darchambeau, F., & Bouillon, S. (2015). The age of river-transported carbon: A global perspective *Global Bigeochem. Cycles, 29*, 122-137. https://doi.org/10.1002/2014GB004911

Mayorga, E., Seitzinger, S. P., Harrison, J. A., Dumont, E., Beusen, A. H. W., Bouwman, A. F., Fekete, B. M., Kroeze, C., & Drecht, G. V. (2010). Global Nutrient Export from WaterSheds 2 (NEWS 2): Model development and implementation. *Environ. Modell. Softw., 25*, 837-853.

Meybeck, M., & Ragu, A. (2012). *GEMS-GLORI world river discharge database*. https://doi.org/10.1594/PANGAEA.804574

Milliman, J. D. (1993). Production and accumulation of calcium carbonate in the ocean: Budget of a nonsteady state. *Global Biogeochem. Cycles, 7*, 927-957.

Naegler, T., Ciais, P., Rodgers, K., & Levin, I. (2006). Excess radiocarbon constraints on air-sea gas exchange and the uptake of CO_2 by the oceans. *Geophys. Res. Lett., 33*, L11802. https://doi.org/10.1029/2005GL025408

Najjar, R. G., Jin, X., Louanchi, F., Aumont, O., Caldeira, K., Doney, S. C., Dutay, J. C., Follows, M., Gruber, N., Joos, F., Lindsay, K., Maier-Reimer, E., Matear, R. J., Matsumoto, K., Monfray, P., Mouchet, A., Orr, J. C., Plattner, G. K., Sarmiento,

J. L., Schlitzer, R., Slater, R. D., Weirig, M. F., Yamanaka, Y., & Yool, A. (2007). Impact of circulation on export production, dissolved organic matter, and dissolved oxygen in the ocean: Results from Phase II of the Ocean Carbon-cycle Model Intercomparison Project (OCMIP-2). *Global Biogeochemical Cycles, 21*(3), n/a-n/a. https://doi.org/10.1029/2006gb002857

Peterson, B. J., & Fry, B. (1987). Stable isotopes in eco-system studies. *Ann. Rev. Ecol. Syst., 18*, 293-320.

Rayner, N. A., Parker, D. E., Horton, E. B., Folland, C. K., Alexander, L. V., Rowell, D. P., Kent, E. C., & Kaplan, A. (2003). Global analyses of sea surface temperature, sea ice, and night marine air temperature since the late nineteenth century. *J. Geophys. Res., 108*(D14), 4407. https://doi.org/10.1029/2002JD002670

Reeburg, W. S. (2007). Oceanic methane biogeochemistry. *Chem. Rev., 107*, 486-513.

Schmittner, A., Gruber, N., Mix, A. C., Key, R. M., Tagliabue, A., & Westberry, T. K. (2013). Biology and air-sea gas exchange controls on the distribution of carbon isotope ratios ($\delta^{13}C$) in the ocean. *Biogeosciences, 10*, 5793–5816.

Sweeney, C., Gloor, E., Jacobson, A. R., Key, R. M., McKinley, G., Sarmiento, J. L., & Wanninkhof, R. (2007). Constraining global air–sea gas exchange for CO_2 with recent bomb ^{14}C measurements. *Global Biogeochem. Cycles, 21*(GB2015). https://doi.org/10.1029/2006GB002784

Wanninkhof, R. (1992). Relationship between wind-speed and gas exchange over the ocean. *J. Geophys. Res., 97*, 7373-7382.

Wanninkhof, R., Asher, W. E., Ho, D. T., Sweeney, C. S., & McGillis, W. R. (2009). Advances in quantifying air-sea gas exchange and environmental forcing. *Annu. Rev. Mar. Sci., 1*, 213-244.

Wanninkhof, R., Park, G.-H., Tankahashi, T., Sweeney, C., Feely, R. A., Nojiri, Y., Gruber, N., Doney, S. C., McKinley, G. A., Lenton, A., Le Quéré, C., Heinze, C., Schwinger, J., Graven, H., & Khatiwala, S. (2013). Global ocean carbon uptake: magnitude, variability and trends. *Biogeosciences, 10*, 1983-2000.

Zhang, J., Quay, P. D., & Wilbur, D. O. (1995). Carbon-isotope fractionation during gas-water exchange and dissolution of CO_2. *Geochim. Cosmochim. Ac., 59*, 107-114.